



Nanoporous gold formation by dealloying: A Metropolis Monte Carlo study



O. Zinchenko, H.A. De Raedt*, E. Detsi, P.R. Onck, J.T.M. De Hosson

Department of Applied Physics, Zernike Institute for Advanced Materials, University of Groningen, Nijenborgh 4, NL-9747 AG, Groningen, The Netherlands

ARTICLE INFO

Article history:

Received 3 December 2012

Received in revised form

30 January 2013

Accepted 5 February 2013

Available online 9 February 2013

Keywords:

Monte Carlo simulation

Nanoporous materials

Catalysts

Sensors

Actuators

ABSTRACT

A Metropolis Monte Carlo study of the dealloying mechanism leading to the formation of nanoporous gold is presented. A simple lattice-gas model for gold, silver and acid particles, vacancies and products of chemical reactions is adopted. The influence of temperature, concentration and lattice defects on the dealloying process is investigated and the morphological properties are characterized in terms of the Euler characteristic, volume, surface area and the specific surface area. It is shown that a minimal three-parameter model suffices to yield nanoporous gold structures which have morphological properties akin to those found in the experiment. The salient features of the structures found by simulation are that the ligament size of the dealloyed material is of the order of 2–3 nm, the structure is disordered, percolating and entirely connected.

© 2013 Elsevier B.V. All rights reserved.

1. Introduction

Sponge-like nanoporous metals with high specific surface area have the potential to outperform existing (dense) materials in various applications, including catalysts [1–3], electrochemical supercapacitors [4,5], biosensors [6], bone tissue engineering [7], heat exchangers and electrochemical actuators [8–12]. In particular, nanoporous metallic materials are very promising as actuation materials. In contrast to polymeric actuators they have higher stiffness and strength and in comparison with piezoelectric ceramics they have less restricted strain amplitudes [9,12]. The mechanical properties of a porous overlayer are very different from the bulk alloy to which it is attached, leading to brittle crack propagation, stress corrosion cracking, and other undesirable materials failure [13]. Fig. 1 shows scanning electron micrographs of a typical dealloyed microstructure (disordered nanoporous gold) at two different magnifications. This nanoporous sample was made by selective dissolution of silver from a 6 carat white gold leaf, i.e. Au₂₅Ag₇₅ (wt%) in concentrated nitric acid (65%) and at room temperature. The open structure is percolating and the ligament spacing is of the order of 10 nm [14–16].

Nanoporous metals are commonly synthesized by dealloying, in which the less noble components of an alloy are chemically or electrochemically dissolved. In the present work we are interested in the formation of disordered nanoporous gold (NPG).

The formation of NPG is often explained in terms of atomic rearrangements at the interface between the metal and the solution. As silver is dissolved, gold atoms are released from surface terraces and they reorganize themselves into clusters [17]. The clusters form the initial surfaces of the ultimately three-dimensionally porous structure, and new gold atoms are supplied to them as dissolution propagates to subsequent atomic layers [17]. Thus, the process is governed by the diffusive redistribution of components on a crystal lattice.

Dealloying processes in alloys are a combination of intricate chemical and physical processes, rendering *first-principle* simulation prohibitively difficult. Therefore, to simulate these processes, simplified models that are amenable to computer simulation have been developed. All these models rely on *ad-hoc* assumptions that serve to make the computational problem tractable. The validity of these assumptions cannot be justified from calculation based on a more fundamental theory and are therefore to be judged on their virtue in (1) reproducing salient features of nanoporous gold and (2) keeping the number of model parameters minimal. Consequently there are several different approaches, each having its strong and weak points, to simulate dealloying. The evolving-surface finite-element method was used by Eilks and collaborators to investigate the dealloying of a binary alloy [18]. A phase field model of diffusion-controlled phase transformation in multi-component systems was studied by Chen and coauthors [19]. Xu and coauthors adopted a level set model for solute precipitation and/or dissolution [20]. Erlebacher and coauthors employed a kinetic Monte Carlo method to study the evolution of nanoporosity during dealloying [21].

* Corresponding author. Tel.: +31 503634852; fax: +31 503634950.
E-mail address: h.a.de.raedt@rug.nl (H.A. De Raedt).

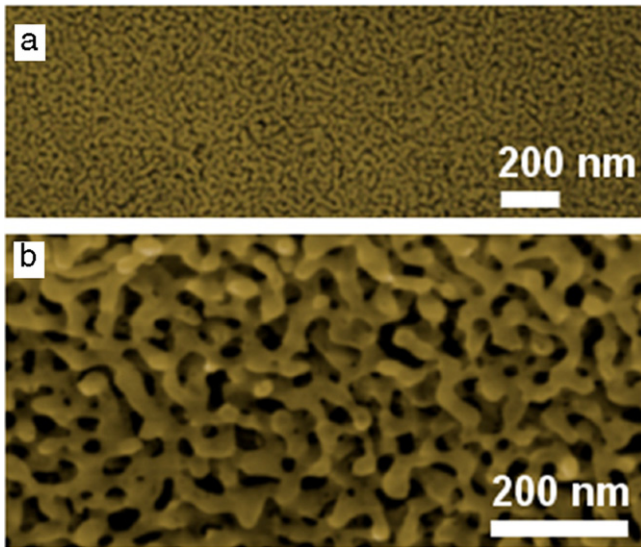
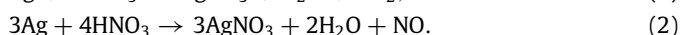
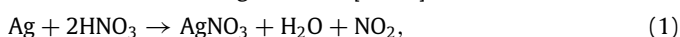


Fig. 1. Scanning electron micrographs of nanoporous gold made by selective dissolution of silver from Au/Ag alloy immersed in nitric acid under free corrosion conditions. (a) Cross-section of dealloyed Au₂₅Ag₇₅ (wt%) thin film. (b) magnification of (a) showing an open structure with ligament spacing of the order of 10 nm.

In the present paper, we use the Metropolis Monte Carlo (MMC) technique to simulate both the chemical reaction processes and the movement of the various particles (gold, silver, acid, reaction products and vacancies). As is well-known [22,23], the motion of the particles in a Monte Carlo simulations is not related to the Newtonian equation of motion, let alone to the time-evolution on the quantum mechanical level. It is therefore dangerous to interpret the transition rates which define the (kinetic or Metropolis) Monte Carlo processes as real physical phenomena that actually occur in Nature. In some cases, it may be possible to give a *statistical* interpretation of what is going on *on average* but the connection to the real-time dynamics of the particles remains elusive. Keeping this in mind, our aim is to construct a simulation technique that captures the main features of the dealloying process and yields configurations of gold particles of which the morphological properties are similar to those of nanoporous gold produced in the laboratory. As the structures obtained by dealloying are irregular in terms of pore and ligament size and are discrete (i.e. represented by a collection of voxels), we characterize the structures using techniques of integral geometry, namely in terms of Minkowski functionals (the Euler characteristic, volume, surface area and mean breadth) [24–27]. This approach does not rely on interpolation techniques to transform binary data into continuous surfaces/densities [15] or digital image processing techniques [16]. For completeness, we mention that in the present work we do study coarsening [28,29] of the structures during annealing.

2. Chemical reactions during dealloying

Dealloying is a common corrosion process during which the most chemically active components of an alloy are selectively dissolved by acid. For the case at hand, disordered nanoporous gold is obtained by dissolving silver atoms from an Au/Ag alloy [21]. The sample of an Au/Ag alloy is put in nitric acid for free corrosion. The mechanism of the formation of sponge-like nanoporous gold is diffusion and clustering of Au atoms while Ag atoms are dissolving [17]. Silver atoms dissolve in nitric acid according to one or both of the following reactions [30,31]:



Products of these reactions are gas (NO or/and NO₂) and liquid (AgNO₃ and H₂O). These reaction products are easily removed from the solid sample.

As the crystal lattice is rigid, one might expect that the pore fraction in NPG reflects the fraction of atoms which are dissolved. However, simultaneous to the creation of porosity, a number of other processes are active, including coarsening behind the dissolution front, various sources of plastic deformation, and capillary forces [32]. As a result, macroscopic volume reduction by as much as 30% during dealloying is observed [32]. In spite of the volume reduction of a sample the specific surface area that we define here as the total surface area per unit of volume, can be large.

3. Model and methods

3.1. Lattice-gas and energy of a particle configuration

Lattice-gas computer simulation models are of wide-spread use for studying of many-particle systems. They allow dealing with a large number of particles at a relatively modest computational cost. The Au/Ag alloy has an FCC structure [33]. Therefore, in the simulation, we work with FCC lattices to represent a 3D structure. Each lattice point of FCC lattice has 12 nearest neighbors and contains only one of the five objects namely Au, Ag, HNO₃, liquid product of the chemical reaction (AgNO₃ or H₂O) and vacancy. In the following, we simply call these objects “particles”. The movement of particles is restricted to exchange between nearest-neighbor positions. This restriction prevents non-physical behavior like jumping of a particle from one edge of the system to another. In other words only nearest neighbor hopping is allowed. Furthermore, this mechanism allows us to simulate the passivation effect during which atoms of gold accumulate on the surface and locally block further dissolution [21]. Another restriction is that solid particles cannot disconnect from the sample through exchange with liquid particles. This restriction together with the clustering mechanism (Section 3.3) guarantees the full integrity of the dealloyed sample.

In the present work we do not take into account the interaction between products of the chemical reaction (AgNO₃ and H₂O) and the “interaction” between vacancies with other particles. The interaction with acid particles yields a more realistic dissolution and diffusion behavior [34]. Therefore we have 9 possible combinations of particles (Ag–Ag, Au–Ag, Ag–Au, Au–Au, Ag–HNO₃, HNO₃–Ag, Au–HNO₃, HNO₃–Au and HNO₃–HNO₃) which contribute to the energy. The energy E of the lattice-gas model with pair potential interactions between nearest-neighbors is given by

$$E = \sum_{\alpha=1}^5 \sum_{\beta=1}^5 \sum_{\langle i,j \rangle} J_{\alpha\beta} M_i^\alpha M_j^\beta + \sum_{\alpha=1}^5 \sum_{i=1}^{L_x L_y L_z} \frac{h_\alpha (z-1)}{(L_z-1)} M_i^\alpha. \quad (3)$$

The variables α and β represent one of five particles: gold ($\alpha, \beta = 1$), silver ($\alpha, \beta = 2$), acid ($\alpha, \beta = 3$), vacancies ($\alpha, \beta = 4$), and reaction products ($\alpha, \beta = 5$). The parameters $J_{\alpha\beta}$ represent the interaction constants between two particles α and β . As $J_{\alpha\beta} = J_{\beta\alpha}$, we have 15 different interaction constants. The notation $\langle i, j \rangle$ indicates that the sum is over nearest-neighbor pairs of the FCC lattice. The variable M_i^α is a binary variable which is equal to one if particle α occupies site i , and is zero otherwise. The dimensions of the lattice are denoted by L_x, L_y and L_z . The chemical potential of particle α is denoted by h_α . In the last sum, the index $i = (x, y, z)$ runs over all sites of the FCC lattice and the symbol z is the index of particle α along the z -axis. Here we assume that the chemical potentials change linearly in the z direction and are uniform in the other two directions, mimicking the effect of an external potential. The first and the second term (see Eq. (3)) represent the interaction

energy and the chemical potential. Our motivation to include the contribution of the chemical potential is to allow us to study the effect of the external field on the dealloying process. Obviously, the number of free parameters in Eq. (3) is large (15) but, as we discuss below, for the present purposes can be reduced to 3.

3.2. Metropolis Monte Carlo

In the present work, all simulations are performed using the MMC method [22,23] and we focus on the properties of the system in thermal equilibrium, not on the kinetics or diffusion of particles which are not incorporated in the MMC scheme. The simulation consists of performing a certain number of Monte Carlo steps to equilibrate the system and then to perform the dealloying simulation. Let us denote a configuration of particles on the lattice by the symbol ξ .

The Metropolis Monte Carlo method is a fairly general algorithm for generating a set of N different configurations $\xi_1, \xi_2, \xi_3, \dots, \xi_N$ of the system such that the frequency, with which a configuration ξ appears, converges to the probability $P(\xi)$. Here $P(\xi)$ is a specified probability distribution. As usual, we assume that the system under study is in equilibrium with its surrounding and therefore $P(\xi)$ is given by

$$P(\xi) = Z^{-1} e^{-E(\xi)/k_B T} = Z^{-1} e^{-\beta E(\xi)}. \quad (4)$$

Here $E(\xi)$ is the energy of the configuration ξ , T is the temperature, $k_B = 1.38 \times 10^{-23} \text{ JK}^{-1}$ is the Boltzmann constant, $\beta = 1/k_B T$, and the partition function Z is given by

$$Z = \sum_{\xi} e^{-\beta E(\xi)}. \quad (5)$$

One Metropolis Monte Carlo step consists of randomly picking a new configuration and accepting or rejecting the new configuration with a prescribed acceptance probability. The initial configuration ξ_1 can be any configuration of the system, e.g., any arrangement of particles in the system. At the n th step the system is in configuration ξ_n . Then the algorithm picks a trial configuration ξ' (usually a configuration which is close to ξ_n) and computes the ratio

$$R = \frac{P(\xi')}{P(\xi_n)} = e^{-\beta(E(\xi') - E(\xi_n))}. \quad (6)$$

A pseudo-random number $0 \leq p < 1$ is generated and if $p \leq R$, the system changes to the configuration ξ' . Otherwise the system remains in the configuration ξ_n . These MMC steps are repeated N times, where N is a sufficiently large number. Note that the probability of accepting a trial configuration ξ' is

$$P_{\xi_n, \xi'} = \begin{cases} e^{-\beta(E(\xi') - E(\xi_n))} & \text{if } E(\xi') - E(\xi_n) > 0 \\ 1 & \text{otherwise.} \end{cases} \quad (7)$$

During a simulation, the total energy of the system is calculated and used to monitor the approach to the equilibrium state.

The proposed MMC model features various input parameters. The parameters that affect the system energy are the temperature T , the pair-wise interactions between nearest-neighbor particles $J_{\alpha\beta}$, the external fields acting on different particles through the chemical potential h_α and the mobility of liquid and solid particles. The temperature directly affects the acceptance probability of the MMC process (see Eq. (7)). The pair-wise interactions between nearest-neighbor particles contribute to the energy of all different pairs of particles (Au–Au, Au–Ag, Ag–Ag, Au–HNO₃, Ag–HNO₃ and HNO₃–HNO₃). The external fields h_α control the chemical potential of Au ($\alpha = 1$), Ag ($\alpha = 2$) and HNO₃ ($\alpha = 3$) particles, respectively. In terms of MMC steps, the mobility of the particles is

controlled through the probability of choosing a liquid versus another particle. In other words, more mobile particles have larger chances for making exchanges with nearest-neighbors. The mobility parameter controls the speed of the corrosion and removal of chemical reaction products.

According to Eq. (3), in the present model there are 15 parameters (10 pair-wise interaction constants $J_{\alpha\beta}$ and 5 constants h_α defining the chemical potential) which enter the expression of total energy of the system. Extensive simulations lead us to the conclusion that for the purposes outlined in the introduction, the model may be simplified significantly. In fact, it turns out that we may assume that $J_{13} = J_{23} = J_{33} = J_{14} = J_{24} = J_{34} = J_{15} = J_{25} = J_{35} = J_{45} = 0$ and $h_1 = h_2 = h_3 = h_4 = h_5 = 0$. In this case, the energy E of the system simplifies to

$$E = \sum_{\alpha=1}^2 \sum_{\beta=1}^2 \sum_{(i,j)} J_{\alpha\beta} M_i^\alpha M_j^\beta. \quad (8)$$

Therefore, the model that we will focus on in the following has only 3 parameters. Our initial choice of these interaction parameters is guided by the work reported in Ref. [35]. One might think that these 3 interaction parameters can be fixed by fitting the phase diagram of the bulk gold–silver alloy to the phase diagram of the simple model Eq. (3), but as we are dealing with rather thin films here and the effect of the electrolyte on the electron density of the alloy (with pores) is not readily incorporated in the J 's, this is by no means evident. Therefore we leave the 3 J 's as free parameters and adjust them until we find NPG structures that are similar to those found in the experiment.

3.3. Chemical reactions and boundary conditions

In the present work we take into account only one of the two possible chemical reactions (see Eq. (1)), the reason being that the second reaction has a smaller probability to occur. This can be seen as follows. Each lattice point of the FCC lattice has 12 nearest neighbor sites, which contains only one of the five different particles. Therefore each lattice site has $5^{12} = 244140625$ different configurations of neighbors. Of all these configurations, 177031761 can lead to reaction Eq. (1) whereas only 29831692 can produce reaction Eq. (2). This means that the probability for reaction Eq. (1) is about 0.73 and for Eq. (2) it is only 0.12. It is more likely that two nitric acid particles would be near a silver particle (Eq. (1)) than 4 nitric acid particles would be near 3 particles of silver (Eq. (2)). Liquid products of the chemical reactions are replaced by new acid particles when they reach a boundary of the sample. Finally, the simulation stops when a certain amount (typically 99%) of silver particles has been dissolved.

The Monte Carlo algorithm that we have described above has an obvious limitation in that it allows for the possibility that clusters of particles become detached from each other. For instance, one can imagine the case in which clusters of particles are connected to each other through a thin silver “wire”. This connection would easily be dissolved by the nitric acid, leaving two disconnected clusters of particles. As our MMC simulation proceeds by moving one particle at a time, it would take a lot of Monte Carlo steps before the two disconnected clusters join again. A nice feature of the MMC method is that it is easy to add moves which involve clusters of particles and therefore speed up this process. Such a clustering mechanism guarantees the integrity of the system and, most importantly, provides a simple mechanism to obtain the experimentally observed shrinkage of the sample [32]. Thus, in the simulation we allow for movements that merge disconnected clusters of particles by moving the smallest cluster to the closest part of the sample, properly weighted by the corresponding Boltzmann factors.

We use periodic boundary conditions in the x and y directions and open boundary condition in the z direction. The flow of acid ions is along the z direction. Thus, our simulation model mimics a quasi-infinite film of Au/Ag alloy immersed in acid.

As the experiment was performed with Au/Ag films, the systems which we simulate are rectangular parallelepipeds. The size dependence of the results was studied by performing numerous tests, using lattice sizes ranging from $100 \times 100 \times 50$ to $300 \times 300 \times 50$. Comparison of the specific surface area, ligament sizes and patterns of the simulated structures shows that there is no significant dependence in this range of system sizes. This allows us to use relatively small systems for the dealloying calculations.

4. Morphological analysis

To characterize the morphology of the gold structures quantitatively we calculated the Minkowski functionals [24,25]. A fundamental theorem in integral geometry [24] states that in three dimensions, there are four Minkowski functionals namely the volume whose morphology is to be determined, the area of the interface separating that volume from the rest of the system, the mean breadth and the Euler characteristic [24,25]. The Euler characteristic (or Euler–Poincaré characteristic) is a topological invariant, a number that describes the topological shape or structure, regardless of the way the structure is bent. Comparison with the experiments is made in terms of the specific surface area, the sample size, the relative size of the ligaments, and two-dimensional projections of the structure itself. The Minkowski functionals are closely related to the principal curvatures of the surfaces of bodies comprising the structure, as defined in differential geometry [24,25]. As in the simulation, the structures are already represented on a discrete lattice, the integral-geometry approach is much easier to use than the corresponding differential-geometry. In practice, we compute the Minkowski functionals using the integral-geometry algorithm described in [26,27].

The first step of calculation is to assign a small cube or sphere to each coordinate (on the FCC lattice) of a solid particle. Next, the algorithm discretizes the resulting structure using a regular cubic lattice with a fine mesh. This results in a 3D image in which some cubes (voxels) are filled and others are not. The final step is to compute the Minkowski functionals of the 3D image on this fine mesh, following the prescription given in [26,27]. In essence, the algorithm is very simple, a direct consequence of the integral-geometry approach. Each filled voxel of the regular cubic lattice is decomposed into disjoint sets of 8 vertices, 12 edges and 6 faces. The morphological characterization of a 3D cubic pattern amounts to the counting of the elementary geometric objects (cubes, vertices, edges and faces) that constitute the 3D image [26,27]. Overlapping vertices, edges or faces of neighboring voxels are counted only once. According to integral geometry, the volume, the surface area and the Euler characteristic are given by

$$V = N_{\text{cub}}, \quad (9)$$

$$S = 2N_{\text{face}} - 6N_{\text{cub}}, \quad (10)$$

$$\chi = N_{\text{face}} + N_{\text{vert}} - N_{\text{cub}} - N_{\text{edge}}, \quad (11)$$

where N_{cub} , N_{face} , N_{vert} , N_{edge} is the total number of elementary cubes, faces, vertices and edges, respectively [26,27]. The specific surface area is defined as

$$A = S/V, \quad (12)$$

and follows directly from Eqs. (9) and (10).

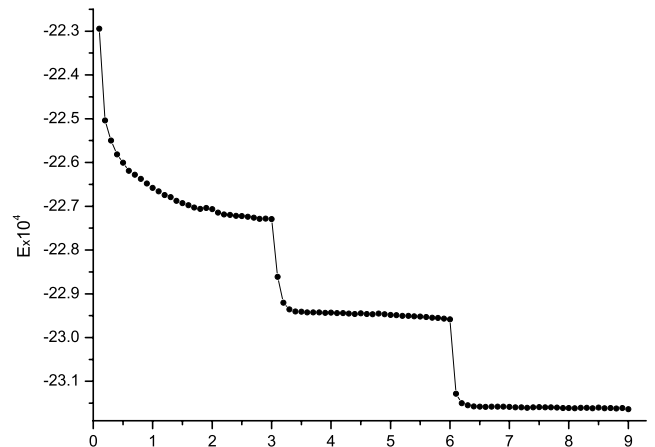


Fig. 2. Relaxation of the total energy E of the system as a function of n , the number of MMC steps per particle. For $n < 3 \times 10^4$, the temperature $T = 500$ K, for $3 \times 10^4 < n < 6 \times 10^4$, the temperature $T = 400$ K and for $n > 6 \times 10^4$, the temperature $T = 300$ K. The plateaus indicate that quasi-equilibrium states were reached. System interaction constants are $J_{11} = 0.047$ eV, $J_{22} = 0.043$ eV, $J_{12} = 0.037$ eV. The system size is $100 \times 100 \times 50$ ($29.1 \times 29.1 \times 14.4$ nm³).

5. Results and discussion

5.1. Equilibration

When the dealloying process is started, we assume that the alloy is in a quasi-equilibrium state. However, the corresponding atomic arrangement is not known a priori. Therefore, in the equilibration process, we take as the initial arrangement a random distribution of particles over the FCC lattice and use the MMC method to find the equilibrium state for the current set of input parameters. Evidently, in this phase of the simulation we do not allow for chemical reaction processes. The relaxation process was performed by gradual cooling down (annealing) to the desired dealloying temperature. This procedure forces the system to change gradually from the initial random rearrangement of atoms (which corresponds to infinite temperature) to an equilibrated state at the temperature at which the dealloying is going to take place. A typical example of cooling a system from infinite temperature down to 300 K is presented in Fig. 2 where we plot the total energy E as a function of the number of MMC cycles per particle n . Three plateaus indicate that three quasi-equilibrium states have been reached, corresponding to the specified temperatures 500 K, 400 K and 300 K respectively. Repeating the equilibration simulation for different choices of the interaction strength between gold and silver yields the “phase diagram” presented in Fig. 3. In this diagram one can clearly see two distinct configurations: the mixed configuration and the clustered configuration.

The evolution of the Euler characteristic and specific surface area of gold structures (disregarding silver) during the relaxation process is shown in Figs. 4 and 5. Two different sets of interaction constants were chosen for these simulations, corresponding to the two different types of equilibrium configurations. Relaxation with one set of interaction constants leaves the system in an atomically mixed configuration (see Fig. 4) and relaxation with another set produces gold clusters immersed in silver (Fig. 5). Atomically mixed configurations yield a negative value of Euler characteristic which is of the order of N_{Au} , number of gold particles in the system. In the case of a clustered configuration the Euler characteristic $\chi \approx N_{\text{Cl}}$, where N_{Cl} is a number of disconnected gold clusters.

Prior to dissolution the alloy must be homogeneous with no phase separation [36]. Porosity evolution thus forms dynamically

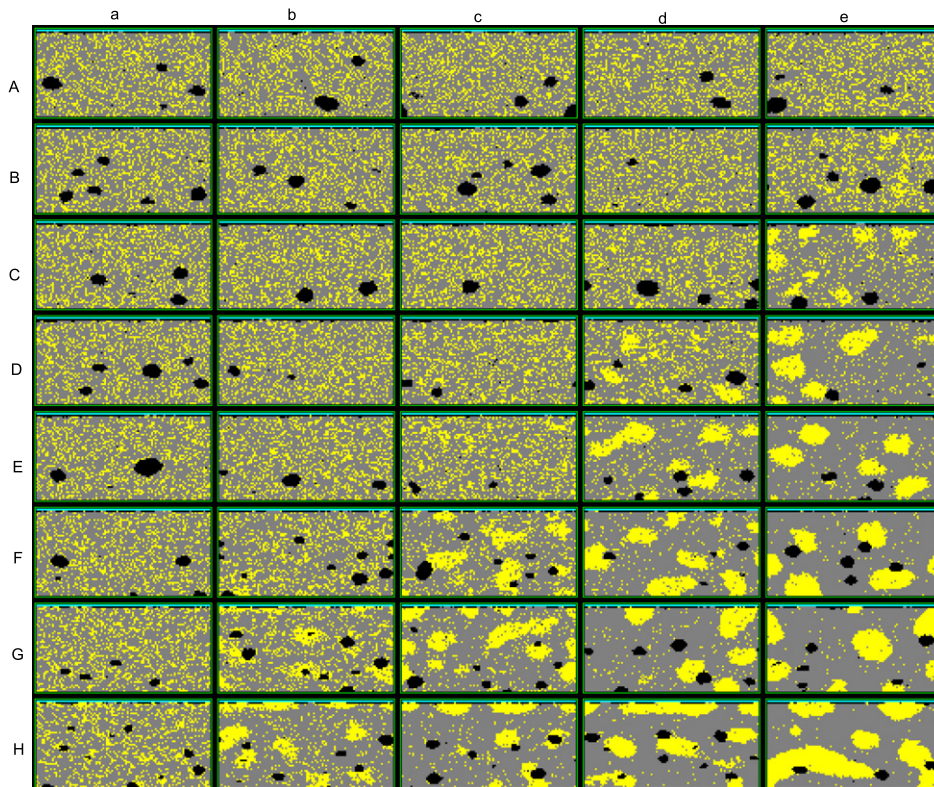


Fig. 3. “Phase diagram” of equilibrated structures. Snapshots of cross sections of the $\text{Au}_{25}\text{Ag}_{75}$ (wt%) systems were taken after equilibration. Yellow: gold; gray: silver; black: vacancies. The gold–gold interaction J_{11} increases from the left column to the right column in the range of [0.045, 0.049] eV in steps of 0.001 eV: for each row, $J_{11} = 0.045$ (a), 0.046 (b), 0.047 (c), 0.048 (d), 0.049 (e). The silver–silver interaction J_{22} increases from the top row to the bottom row in the range of [0.035, 0.049] eV in steps of 0.002 eV: for each column, $J_{22} = 0.035$ (A), 0.037 (B), 0.039 (C), 0.041 (D), 0.043 (E), 0.045 (F), 0.047 (G), 0.049 (H). The gold–silver interaction J_{12} decreases from the left column to the right column in the range of [0.039, 0.035] eV in steps of 0.001 eV: for each row, $J_{12} = 0.039$ (a), 0.038 (b), 0.037 (c), 0.036 (d), 0.035 (e). The temperature $T = 300$ K. The system sizes are $100 \times 100 \times 50$ ($29.1 \times 29.1 \times 14.4 \text{ nm}^3$). (For interpretation of the references to colour in this figure legend, the reader is referred to the web version of this article.)

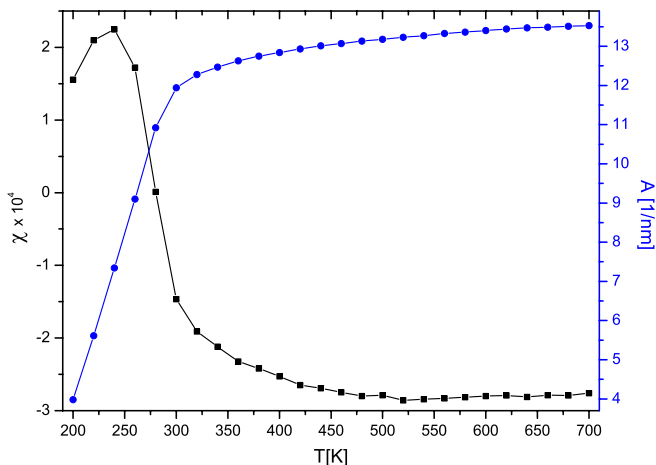


Fig. 4. The Euler characteristic χ (squares) and the specific surface area A (circles) of gold particles as a function of a temperature T . The negative values of the χ indicate that gold particles mix with silver. The sharp drop in χ signals the transition into mixed configurations. The largest value of the specific surface area A corresponds to the most mixed system. Near the temperature $T = 250$ K, a transition from a clustered configuration to a mixed configuration is observed. System interaction constants are $J_{11} = 0.047$ eV, $J_{22} = 0.043$ eV, $J_{12} = 0.037$ eV. The system sizes are $100 \times 100 \times 50$ ($29.1 \times 29.1 \times 14.4 \text{ nm}^3$).

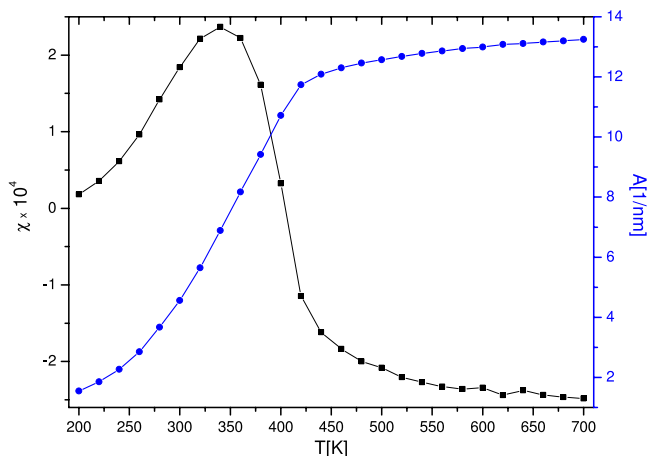


Fig. 5. The Euler characteristic χ (squares) and the specific surface area A (circles) of gold particles as a function of a temperature T . The largest value of χ corresponds to the configuration with the largest amount of disconnected gold clusters. The largest value of a specific surface area A corresponds to the most mixed system. Near the temperature $T = 400$ K, a transition from a clustered configuration to a mixed configuration is observed. System interaction constants are $J_{11} = 0.049$ eV, $J_{22} = 0.044$ eV, $J_{12} = 0.035$ eV. The system sizes are $100 \times 100 \times 50$ ($29.1 \times 29.1 \times 14.4 \text{ nm}^3$).

5.2. Dealloying

The relaxation process changes the infinite temperature (random) configuration of the gold and silver atoms into a typical equilibrium configuration at the temperature at which

during dissolution and is not due to one phase simply being excavated out of the two-phase material [36]. Therefore, interaction constants which lead to clustered configurations may be excluded from further considerations.

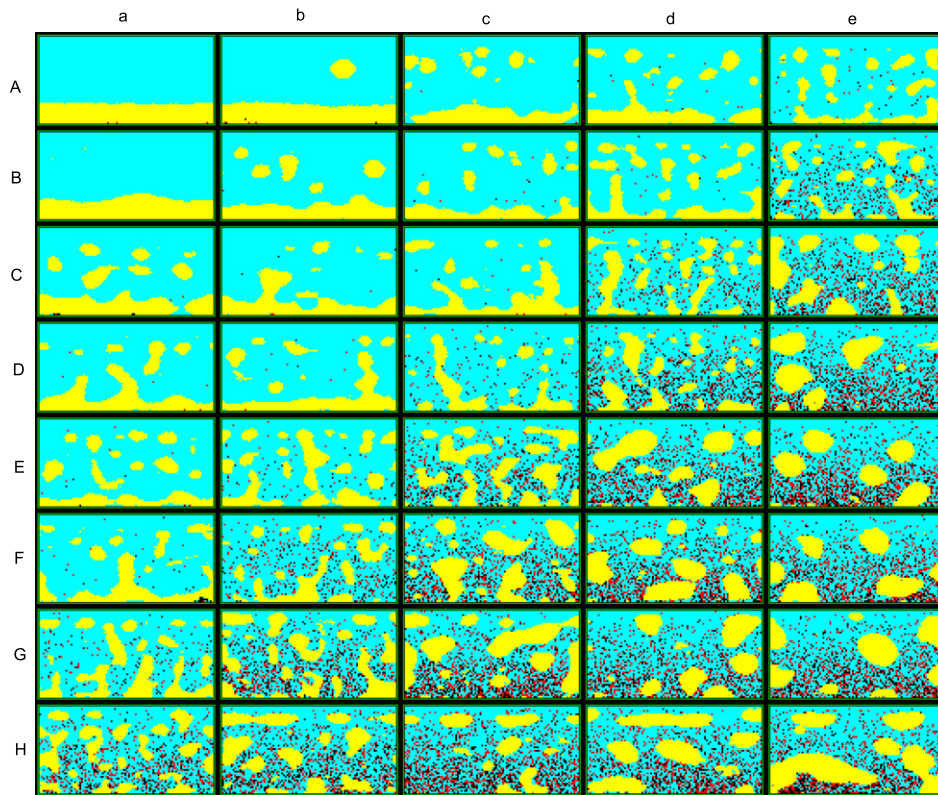


Fig. 6. “Phase diagram” of dealloyed structures. Snapshots of cross sections of the $\text{Au}_{25}\text{Ag}_{75}$ (wt%) dealloyed systems. Yellow: gold; gray: silver; red: products of chemical reactions; black: vacancies. The gold–gold interaction J_{11} increases from the left column to the right column in the range of [0.045, 0.049] eV in steps of 0.001 eV: for each row, $J_{11} = 0.045$ (a), 0.046 (b), 0.047 (c), 0.048 (d), 0.049 (e). silver–silver interaction J_{22} increases from the top row to the bottom row in the range of [0.035, 0.049] eV in steps of 0.002 eV: for each column, $J_{22} = 0.035$ (A), 0.037 (B), 0.039 (C), 0.041 (D), 0.043 (E), 0.045 (F), 0.047 (G), 0.049 (H). The gold–silver interaction J_{12} decreases from the left column to the right column in the range of [0.039, 0.035] eV in steps of 0.001 eV: for each row, $J_{12} = 0.039$ (a), 0.038 (b), 0.037 (c), 0.036 (d), 0.035 (e). The temperature $T = 300$ K. The system sizes are $100 \times 100 \times 50$ ($29.1 \times 29.1 \times 14.4$ nm³). (For interpretation of the references to colour in this figure legend, the reader is referred to the web version of this article.)

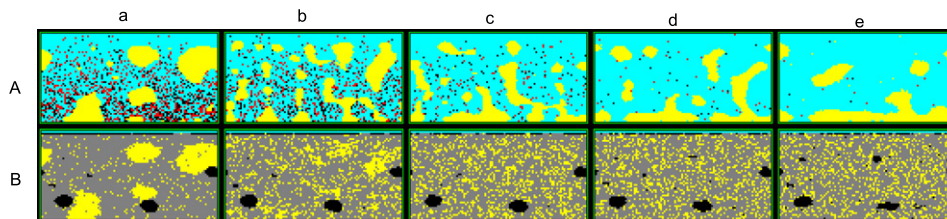


Fig. 7. Snapshots of cross sections of equilibrated structures of the $\text{Au}_{25}\text{Ag}_{75}$ (wt%) sample (B) and corresponding dealloyed structures (A) for different temperatures. The temperature increases from the left column to the right column in the range of [200, 400] K in steps of 50 K: for each row, $T = 200$ K (a), 250 K (b), 300 K (c), 350 K (d), 400 K (e). Yellow: gold; gray: silver; black: vacancies; red: products of chemical reactions; cyan: nitric acid. System interaction constants are $J_{11} = 0.047$ eV, $J_{22} = 0.043$ eV, $J_{12} = 0.037$ eV. The system sizes are $100 \times 100 \times 50$ ($29.1 \times 29.1 \times 14.4$ nm³). (For interpretation of the references to colour in this figure legend, the reader is referred to the web version of this article.)

the dealloying is going to take place. To start the dealloying, the only change to the Monte Carlo algorithm is the inclusion of the chemical reaction processes. The simulation of the dealloying is performed using the same set of model parameters J_{11} , J_{12} and J_{22} as in the equilibration process. The fact that in the simplified model Eq. (8), there is no nearest-neighbor interaction between acid and metal particles does not prevent a chemical reaction between these particles to take place. Indeed, by construction, in the Monte Carlo algorithm such reactions can take place whenever silver and acid particles are nearest neighbors.

A “phase diagram” of dealloyed structures is presented in Fig. 6. In this diagram one can distinguish three distinct configurations - configurations with gold clusters that accumulated mostly in the bottom of the sample (e.g. the system with $J_{11} = 0.045$ eV, $J_{22} = 0.035$ eV, $J_{12} = 0.039$ eV, $T = 300$ K), configurations with disordered NPG (e.g. the system with $J_{11} = 0.047$ eV, $J_{22} = 0.043$ eV,

$J_{12} = 0.037$ eV, $T = 300$ K) and configurations which correspond to clustered equilibrated configurations (e.g. the system with $J_{11} = 0.049$ eV, $J_{22} = 0.049$ eV, $J_{12} = 0.035$ eV, $T = 300$ K). Simulations with different temperatures produce distinct structures (see Fig. 7) that exhibit all of the three “phases”.

Comparing the two “phase diagrams” (Figs. 3 and 6), we may conclude that the NPG structures can only be obtained within a narrow range of interaction parameters. Within this range, these structures are robust to changing of interaction parameters.

The evolution of the Euler characteristic and the specific surface area of gold particles during the dealloying process are shown in Fig. 8. The plateau-like regions in Fig. 8 correspond to the stage when acid reaches the bottom of the sample. The constant Euler characteristic during this stage is due to the fact that the system exhibits percolation. In this stage, creating additional holes in the system is very difficult. The slow decrease of a specific surface area

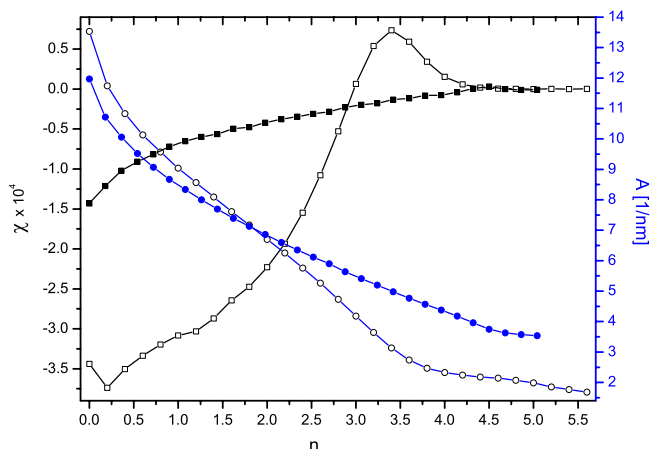


Fig. 8. The Euler characteristic χ (squares) and the specific surface area A (circles) of gold particles as a function of n , the number of MMC steps per particle. The constant Euler characteristics χ during the final stage indicate that the systems are percolating. The slow decrease of A at the final stage of the simulation is due to further equilibration of the samples. Solid squares and circles: $J_{11} = 0.047$ eV, $J_{22} = 0.043$ eV, $J_{12} = 0.037$ eV, $T = 300$ K. Open squares and circles: $J_{11} = 0.046$ eV, $J_{22} = 0.035$ eV, $J_{12} = 0.038$ eV, $T = 300$ K. The system sizes are $100 \times 100 \times 50$ ($29.1 \times 29.1 \times 14.4$ nm³).

A with the increasing number of MMC steps is due to annealing of the sample.

First, we present some examples of 2D slices of the system during the dealloying process; see Fig. 9. The 3D picture of the dealloyed sample, the results of the analysis of the geometry of dealloyed structure and simulation parameters are shown in Fig. 10. Several bottom layers of the dealloyed system contain enhanced amounts of gold particles due to the boundary condition in this direction (Fig. 9(d)). Qualitatively, the pattern of the simulated system (see Fig. 11) is similar to the microscopy picture of the dealloyed sample (see Fig. 1(b)). From the 2D snapshot of the equilibrated system (see Fig. 9(a)) and the behavior of the Euler characteristic (see Fig. 4) we may conclude that gold (yellow) and silver (gray) are entirely mixed. Vacancies (black) in the sample are represented by voids that are randomly located in the initial configuration. During the equilibration, the vacancies merge into “clusters” (Fig. 9(a)). During the dealloying, vacancies can only appear as the result of the chemical reactions Eq. (1). In this reaction, three particles are converted into two particles and one gas molecule. The latter is not explicitly taken into account

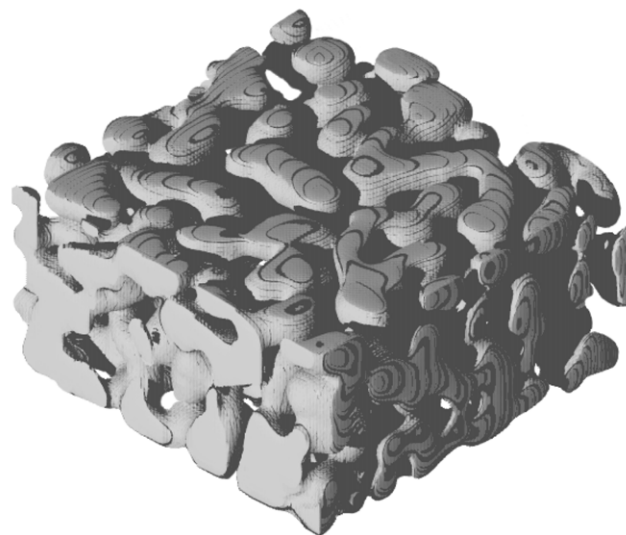


Fig. 10. Typical distribution of the nanoporous structure as obtained by simulating chemical dealloying of an Au/Ag sample. View from the “top” of the dealloyed system. $J_{11} = 0.047$ eV; $J_{22} = 0.043$ eV; $J_{12} = 0.037$ eV; $T = 300$ K. The system size is $100 \times 100 \times 50$ ($29.1 \times 29.1 \times 14.4$ nm³). Volume of the system $V = 4524.0$ nm³. Surface area $S = 14663.9$ nm². Specific surface area $A = 3.24$ 1/nm. The Euler characteristic $\chi = 46$. The ligament size is of the order of 2–3 nm.

in the simulation. Phrased differently, our simulation does not distinguish between true vacancies and sites occupied by a gas molecule. The dealloying process is stopped when 99% of the initial amount of silver was dissolved. The dealloyed structure is entirely connected.

6. Conclusions

In the present paper, we have studied the chemical dealloying by means of Metropolis Monte Carlo simulations. As a model system, we considered Au/Ag alloys immersed in nitric acid.

The simulation of dealloying process was made in two stages: equilibration (Section 5.1) and dealloying (Section 5.2). The first stage allowed us to exclude ranges of model parameters which lead to equilibrated systems which are not found in the experiment, still leaving a huge space of physically acceptable interaction parameters to explore. In the second stage, we excluded interaction parameters which lead to configurations with

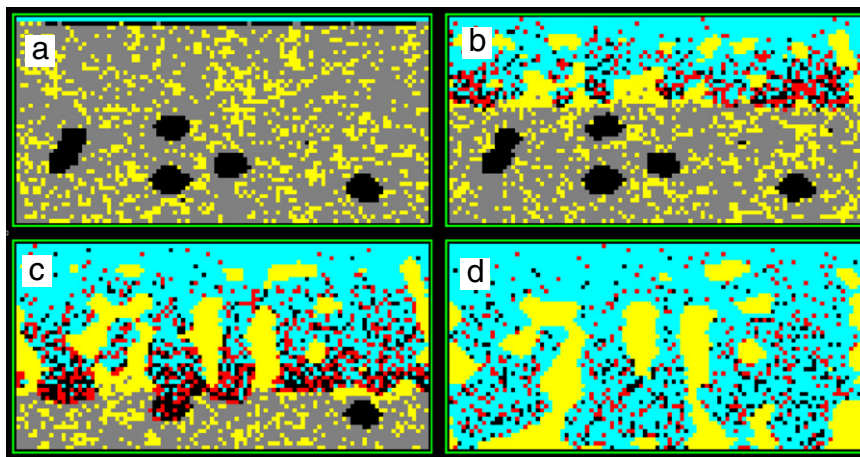


Fig. 9. Snapshots of cross sections of the Au₂₅Ag₇₅ (wt%) sample taken during the MMC simulation after n MMC steps per particle. Yellow: gold; gray: silver; black: vacancies; red: products of chemical reactions; cyan: nitric acid. **a:** $n = 0$; **b:** $n = 5 \times 10^2$; **c:** $n = 2 \times 10^3$; **d:** $n = 6 \times 10^3$. System interaction constants are $J_{11} = 0.047$ eV, $J_{22} = 0.043$ eV, $J_{12} = 0.037$ eV. The temperature $T = 300$ K. The system size is $100 \times 100 \times 50$ ($29.1 \times 29.1 \times 14.4$ nm³). (For interpretation of the references to colour in this figure legend, the reader is referred to the web version of this article.)

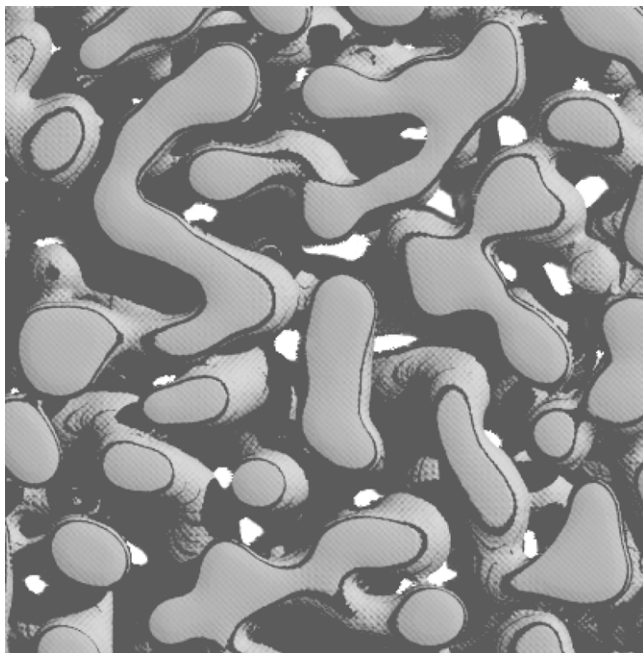


Fig. 11. Plane cut taken from the system shown in Fig. 10, showing the typical distribution of gold particles as obtained by simulating chemical dealloying of an Au/Ag sample.

gold clusters that accumulated mostly at the bottom of the sample. As a result, only a narrow range of interaction parameters yields acceptable physically realistic structures. All these structures are robust to changes of the interaction parameters within this range.

A relevant conclusion in relation to experiments is that simulations provide insight in the processing–structure relationship. Essential parameters turn out to be the Au fractions, the chemical potentials for the acid ions and the vacancy concentrations. The structures of the nanoporous gold are found to be robust to changes of all these parameters provided these are in a particular range. In case of robustness the Au fractions are ranging between 20% and 30%, the chemical potentials for the acid ions between 0 and 0.1 eV and the vacancy concentration in the range up to 10.

Further, the salient features of the structures found by simulation are that the ligament size of dealloyed material is of the order of 2–3 nm, the structure is disordered, percolating and entirely connected. Compared to the initial volume of the system, the dealloying process leads to a reduction of the film thickness by about 10%. The specific surface area of simulated structure $A = 3.24 \text{ 1/nm}$ corresponds to the specific surface area which was calculated analytically for the random structure with ligament diameter of 1.14 nm [37].

Acknowledgments

The authors are grateful to The Netherlands Organization for Scientific Research (NWO-The Hague, Mozaiek 2008 BOO Dossier nr: 017.005.026) and the Zernike Institute for Advanced Materials for financial support.

References

- [1] A. Wittstock, V. Zielasek, J. Biener, C. Friend, M. Baumer, *Science* 327 (2010) 319.
- [2] L. Nagle, J. Rohan, *Int. J. Hydrog. Energy* 36 (2011) 10319.
- [3] C. Xu, X. Xu, J. Su, Y. Ding, J. Catal. 252 (2007) 243.
- [4] X. Lang, H. Yuan, Y. Iwasa, M. Chen, *Scr. Mater.*
- [5] H. Liu, G. Zhu, *J. Power Sources* 171 (2007) 1054.
- [6] K. Hu, D. Lan, X. Li, S. Zhang, *Anal. Chem.* 80 (2008) 9124.
- [7] T.D.E.E.L. Swan, K.C. Papat, *Biomaterials* 26 (2005) 1969.
- [8] J. Weissmuller, R. Viswanath, D. Kramer, P. Zimmer, R. Wurschum, H. Gleiter, *Science* 300 (2003) 312.
- [9] H. Jin, X. Wang, S. Parida, K. Wang, M. Seo, J. Weissmuller, *Nano Lett.* 10 (2010) 187.
- [10] J. Biener, A. Wittstock, L. Zepeda-Ruiz, M. Biener, V. Zielasek, D. Kramer, et al., *Nature Mater.* 8 (2009) 47.
- [11] H. Jin, J. Weissmuller, *Adv. Eng. Mater.* 12 (2010) 714.
- [12] E. Detsi, S. Punzhin, J. Rao, P.R. Onck, J.T.M. De Hosson, *ACS Nano* 6 (2012) 3734.
- [13] R. Li, K. Sieradzki, *Phys. Rev. Lett.* 68 (1992) 1168.
- [14] H. Rösner, S. Parida, D. Kramer, C. Volkert, J. Weismüller, *Adv. Eng. Mater.* 9 (2007) 535.
- [15] T. Fujita, L.-H. Qian, K. Inoke, J. Erlebacher, M.-W. Chen, *Appl. Phys. Lett.* 92 (2008) 251902.
- [16] J. Wang, R.Z.J. Xia, Y. Ding, X. Zang, Y. Chen, *J. Mater. Sci.* 47 (2012) 5013.
- [17] J. Erlebacher, K. Sieradzki, *Scr. Mater.* 49 (2003) 991.
- [18] C. Eilks, C. Elliot, *J. Comput. Phys.* 227 (2008) 9727.
- [19] Q. Chen, N. Ma, K. Wu, Y. Wang, *Scr. Mater.* 50 (2004) 471.
- [20] Z. Xu, H. Huang, X. Li, P. Meakin, *Comput. Phys. Comm.* 183 (2012) 15.
- [21] J. Erlebacher, M. Aziz, A. Karma, N. Dimitrov, K. Sieradzki, *Nature* 410 (2001) 450.
- [22] D. Landau, K. Binder, *Monte Carlo Simulations in Statistical Physics*, Cambridge University Press, 2000.
- [23] M. Newman, G. Barkema, *Monte Carlo Methods in Statistical Physics*, Oxford: Clarendon press, 1999.
- [24] H. Hadwiger, *Vorlesungen ber Inhalt. Oberfläche und Isoperimetrie*, Springer Verlag, Berlin, 1957.
- [25] L. Santalo, *Integral Geometry and Geometric Probability*, Addison-Wesley, 1976.
- [26] K. Michielsen, H. De Raedt, J.T.M. De Hosson, *Adv. Image Electr. Phys.* 125 (2002) 119.
- [27] K. Michielsen, H. De Raedt, *Integral-geometry morphological image analysis*, *Phys. Rep.* 347 (2001) 461.
- [28] J. Erlebacher, *Phys. Rev. Lett.* 106 (2011) 225504.
- [29] K. Kolluri, M. Demkowicz, *Acta Mater.* 59 (2011) 7645.
- [30] A. Groysman, *Corrosion for Everybody*, Springer, 2009.
- [31] R. Maurice, F. Norris, K. Ray, *Living chemistry*, Ginn, 1955.
- [32] S. Parida, D. Kramer, C. Volkert, H. Rosner, J. Erlebacher, J. Weissmuller, *Phys. Rev. Lett.* 97 (2006) 035504.
- [33] S. Kakani, A. Kakani, *Material Science*, New Age International Publishers, 2006.
- [34] S.A. Policastro, R.G. Kelly, J.C. Carnahan, E. Carson, P.F. Reynolds Jr., 212th Electrochemical Society Meeting MA2007-02, 949 (2007).
- [35] M. Gimenez, A. Ramirez-Pastor, E. Leiva, *Surf. Sci.* 600 (2006) 4741.
- [36] J. Erlebacher, *J. Electrochem. Soc.* 151 (2003) C614.
- [37] E. Detsi, E.D. Jong, A. Zinchenko, Z. Vucovic, I. Vucovic, S. Punzhin, K. Loos, G. ten Brinke, H. De Raedt, P.R. Onck, J.T.M. De Hosson, *Acta Mater.* 59 (2011) 7488.